

Article

PdO/ZnO@mSiO₂ Hybrid Nanocatalyst for Reduction of Nitroarenes

Jinwoo Kim, Aram Kim, Nallal Muthuchamy  and Kang Hyun Park * 

Department of Chemistry, Pusan National University, Busan 46241, Korea; nature@chemistry.or.kr (J.K.); aramchemi@gmail.com (A.K.); muthuchamyn89@gmail.com (N.M.)

* Correspondence: chemistry@pusan.ac.kr; Tel.: +82-51-510-2238

Received: 27 June 2018; Accepted: 11 July 2018; Published: 14 July 2018



Abstract: Development of a novel approach for synthesizing nanostructured catalysts and achieving further improvements in catalytic activity, effectiveness, and efficiency remains a major challenge. In this report, we describe the preparation of a nanostructured PdO/ZnO@mSiO₂ hybrid nanocatalyst featuring well-dispersed PdO nanoparticles within hollow ZnO@mSiO₂. The as-prepared PdO/ZnO@mSiO₂ hybrid nanocatalyst exhibited good morphological features, derived from the controlled stepwise synthesis from Pd/PS@ZIF-8@mSiO₂ (PS = polystyrene). The morphology, size, oxidation state, crystallinity, and thermal stability of the prepared PdO/ZnO@mSiO₂ hybrid nanocatalyst were confirmed by a series of physicochemical techniques. The PdO/ZnO@mSiO₂ hybrid nanocatalyst showed very high catalytic efficiency in the reduction of 4-nitrophenol and various nitroarenes under eco-friendly conditions. Therefore, the PdO/ZnO@mSiO₂ hybrid nanocatalyst is a promising alternative catalyst for applications in environmental remediation.

Keywords: nanocatalyst; heterogeneous catalyst; PdO/ZnO; nitrocompound reduction

1. Introduction

Recently, nanoparticles (NPs) have been implicated in important roles and potential applications in diverse research fields, including electrocatalysis, gas-phase catalysis, photocatalysis, sensing, biomedicine, optics, energy conversion and storage, and environmental applications [1–7]. The rising growth and expansion of NP applications has been accompanied by the development of advanced methods based on NPs with unique properties, such as morphology, size, shape, crystallinity, composition, and surface engineered structures [8]. A literature survey shows that metal NPs (MNPs) prepared from inexpensive and earth-abundant metals have attracted attention because of their importance as viable alternatives to expensive and rare noble-metal catalysts. These MNPs often exhibit higher activity than that of the corresponding bulk materials owing to the dissimilar physical and chemical natures, which gives rise to major distinctive properties. Among the MNP catalysts, palladium, zinc, and the corresponding oxide-based MNPs have been extensively studied as catalysts because of their high activity in various reactions [9–12]. The catalytic activity of these structures is highly dependent on their specific morphological properties. Moreover, the development of small nanoscale catalysts on catalytic supports has attracted considerable attention [13].

Various supporting materials have been developed and effectively utilized to load MNPs as catalysts for organic reactions, including Ni-Pd/CB [14], Cu@Cu₂O core-shell nanocatalysts [15,16], Ni-doped Pd-Fe₃O₄ [4], Ag(E)-SiO₂ [17], Pd@pSiO₂ yolk-shell nanoparticles [18], and TiO₂(G)NW@PAPBA-Au HJNH [19]. Silica microspheres (mSiO₂) have been utilized as supports in the research field of core-shell materials as they have many advantages, including simplicity of preparation through known synthetic methods, narrow size distribution, and wide availability from commercial sources [20]. SiO₂-supported nanocatalysts have received special attention in catalytic applications because of their high thermal

stability and tolerance to acidic conditions [17,21,22]. These SiO₂-supported nanocatalysts confer high specific surface areas to SiO₂, leading to uniform dispersion of the catalytic sites, thus preventing aggregation of the MNPs and improving the catalytic activity [23]. However, poor accessibility to these active sites inside the hollow pores limits their catalytic potential, where substantial mass transport is needed. Therefore, SiO₂ supports with easily accessible high surface areas that are not derived from pores are strongly desirable.

Nitrophenol (NP) is widely used in leather coloring agents, dyes, and medicine synthesis. NP is generated as a byproduct during the formulation or photodegradation of pesticides that contain the NP moiety. NP is the most refractory water pollutant with high toxicity and is carcinogenic. In particular, 4-nitrophenols (4-NP) in water pose a significant public health and environmental hazard because of their high solubility and stability in water. For these reasons, 4-NPs are listed as priority organic pollutants by the United States Environmental Protection Agency (US EPA-2008) [24]. Among the various approaches for 4-NP removal, the catalytic reduction of 4-NP to 4-aminophenol (4-AP) is most widely utilized, where the final product is a useful compound in the pharmaceutical industry.

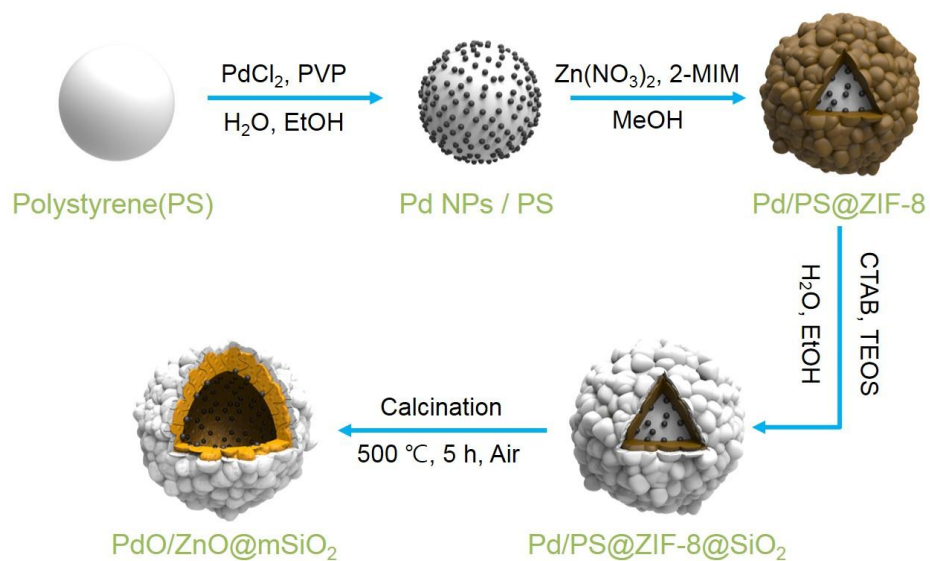
Herein, in an attempt to prepare a heterogeneous PdO/ZnO@mSiO₂ hybrid nanocatalyst for the catalytic degradation of nitroarenes, a Pd/PS@ZIF-8@mSiO₂ nanocomposite (PS = polystyrene) is initially prepared using a uniform coating of mSiO₂ on Pd/PS@ZIF-8 by a sol-gel process; this process is promising for preventing aggregation of the NPs and the nanocatalyst. Pd/PS@ZIF-8@mSiO₂ is then transformed to a PdO/ZnO@mSiO₂ hybrid nanocatalyst by removal of the polystyrene spheres, followed by calcination. In our previous work, we prepared a surfactant-free Pd@pSiO₂ yolk-shell nanocatalyst for the selective oxidation of alcohols [18]. Here, the PdO/ZnO@mSiO₂ hybrid nanocatalyst is used in the effective catalytic reduction of 4-NP and various nitroarenes under eco-friendly conditions.

2. Results and Discussion

2.1. Preparation and Characterization of PdO/ZnO@mSiO₂ Hybrid Nanocatalyst

The PdO/ZnO@mSiO₂ hybrid nanocatalyst was prepared by a stepwise process, as shown in Scheme 1. Firstly, carboxylate-terminated polystyrene spheres (PS spheres) were prepared according to a previously described method [25,26]. Figure 1a,b show the scanning electron microscopy (SEM) images of the PS spheres, illustrating the spherical shape with a smooth surface and monodisperse size distribution. The size distribution in Figure 1c clearly shows that the PS spheres had an average size of around 315 nm. The PS spheres were copolymerized with acrylic acid, resulting in the functionalization of the surface with carboxylic groups to facilitate coordination with metal ions and metal particles [25,26]. The presence of the carboxyl group on the PS surface was confirmed by FT-IR spectroscopy (Figure 1d). The FT-IR spectrum of the PS spheres displayed characteristic peaks at 3200–3600 cm⁻¹ (hydroxyl stretching) and 1730 cm⁻¹ (carboxyl C=O stretching).

For deposition of the Pd nanoparticles on the PS spheres, PdCl₂ was added to the PS sphere dispersion as a metal precursor and NaBH₄ solution was used as a reducing agent. The Pd(II) ions were easily attracted to the surfaces of PS spheres through electrostatic interaction, and after heating the system, the Pd(II) ions were reduced to Pd(0) by polyvinylpyrrolidone (PVP). Figure 2a,b show the SEM images of the palladium nanoparticles deposited on the PS spheres (Pd/PS). After introduction of the Pd nanoparticles, the size and shape of the PS spheres did not change compared to those of the initial PS spheres. The existence of Pd nanoparticles on the PS spheres was confirmed by energy dispersive spectroscopy (EDS) and X-ray powder diffraction (XRD) analysis. The EDS data (Figure 2c) confirmed the presence of Pd. Moreover, intense peaks were observed at 39° and 45° in the XRD patterns (Figure 2d). The peaks were well matched with the (111) and (200) reflections of the face-centered cubic (fcc) structure of Pd (JCPDS No. 46-1043), confirming formation of the Pd nanoparticles.



Scheme 1. Synthetic route for the PdO/ZnO@mSiO₂ hybrid nanocatalyst.

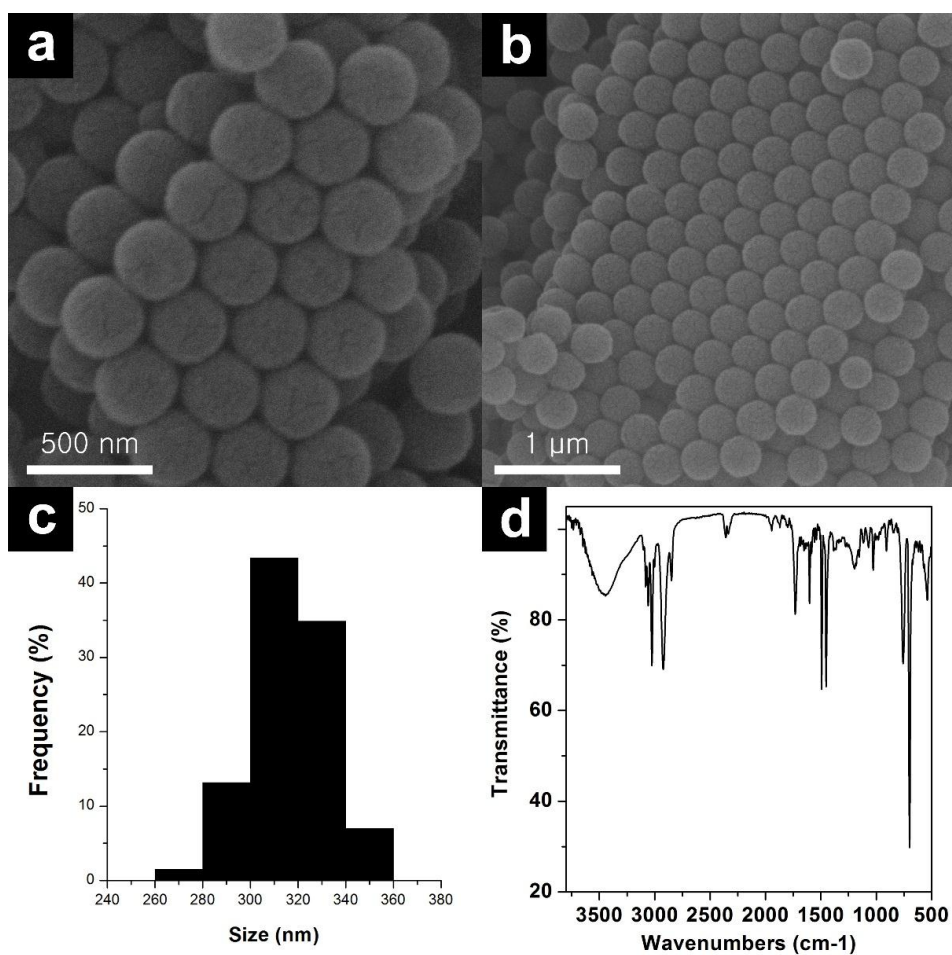


Figure 1. SEM images (a,b); size distribution (c) and FT-IR spectra (d) of PS spheres.

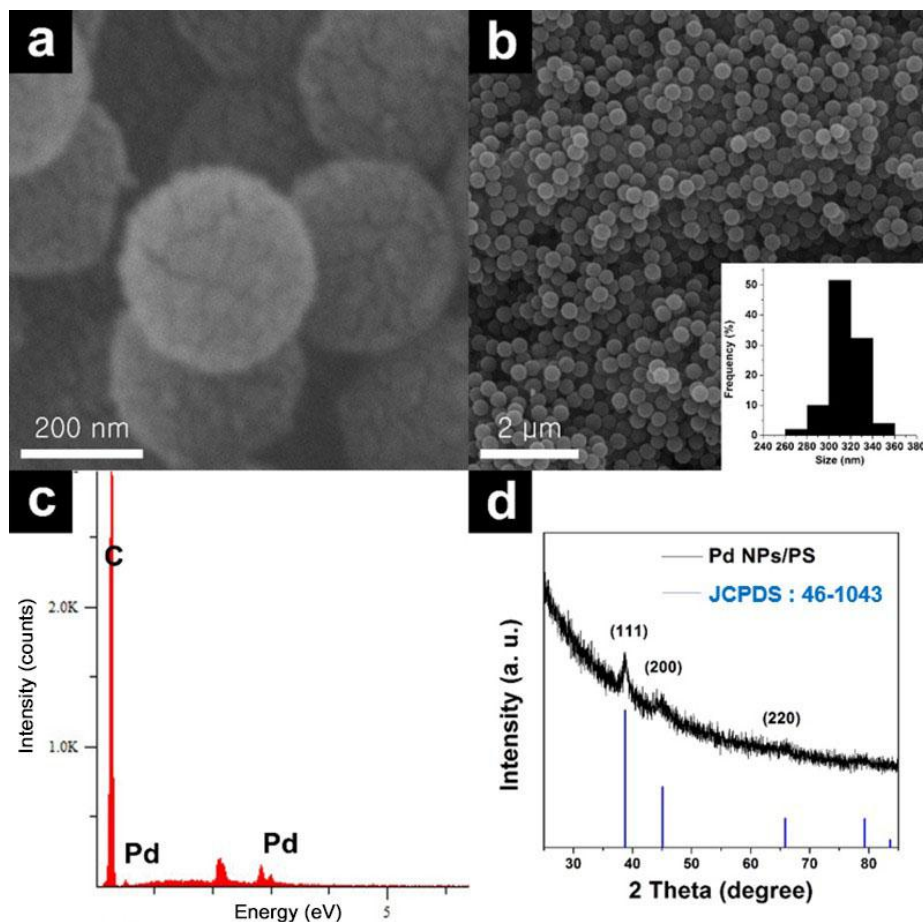


Figure 2. High- and low-resolution (a,b) SEM images of Pd/PS spheres. EDS spectrum (c) and XRD patterns (d) of Pd/PS spheres. The insert in (b) is the size distribution of Pd/PS spheres.

The Pd/PS@ZIF-8 core-shell nanocomposite was prepared by a solvothermal approach. The Pd/PS spheres were added to a precursor methanol solution containing 2-methylimidazole as a ligand and zinc nitrate as a metal precursor to form a zeolitic imidazolate framework (ZIF-8). The carboxylate groups on the surfaces of the PS spheres interacted with the Zn(II) ions and initiated the growth of ZIF-8 on the surfaces of the PS spheres. The SEM images in Figure 3a,b clearly show the monodisperse Pd/PS@ZIF nanocomposite with a change in the size from 315 to 370 nm, indicating the formation of ZIF-8 shells with a thickness of 27.5 nm surrounding the Pd/PS nanocomposite during the growth of ZIF-8. The ZIF-8 shell made the surface of the Pd/PS@ZIF-8 nanocomposite rougher than the surface of the Pd/PS nanocomposite (see inset in Figure 3a). This is attributed to the growth of nanoscale ZIF-8 on the Pd/PS nanocomposite. The elemental composition of the Pd/PS@ZIF-8 nanocomposite was determined using EDS, illustrating peaks of carbon, zinc, and palladium (Figure 3c). A significant amount of the carbon is derived from the polystyrene core. The composition of the ZIF-8 shell was also examined using XRD (Figure 3d). The XRD pattern of the ZIF-8 shell matched well with the XRD pattern of pure sodalite ZIF-8 nanocrystals [27].

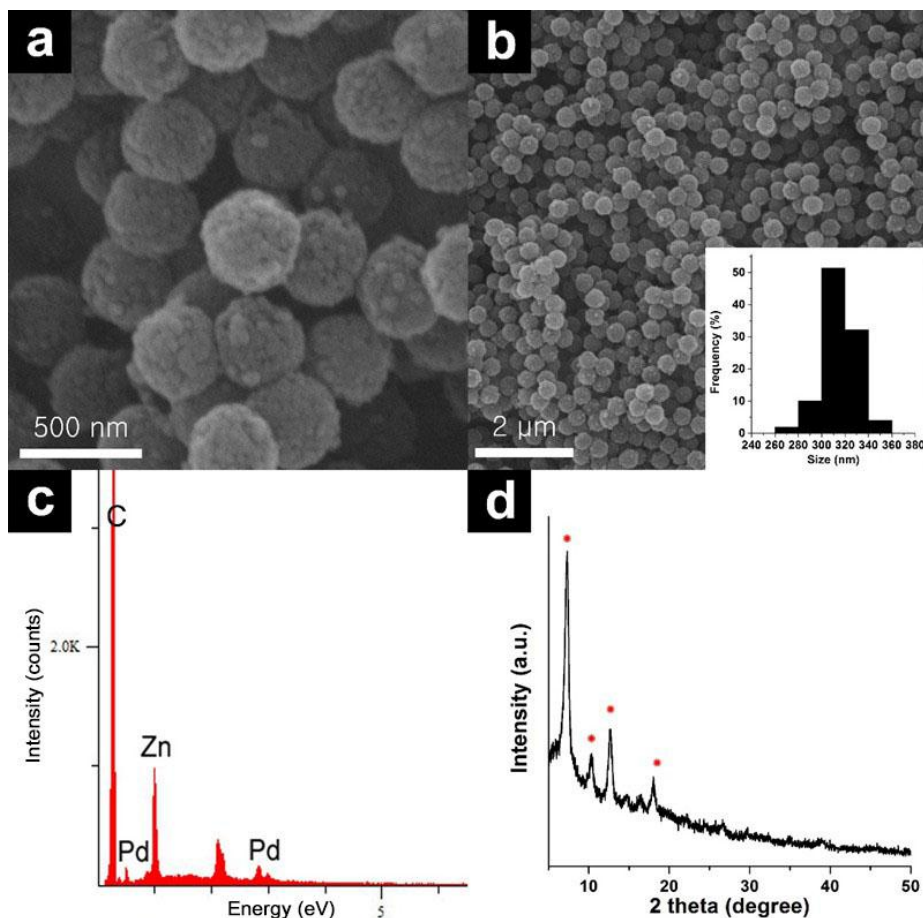


Figure 3. SEM images (a,b); EDS spectrum (c) and XRD patterns (d) of Pd/PS@ZIF-8 core-shell nanocomposites. The insert in (b) is the size distribution of Pd/PS@ZIF-8 core-shell nanocomposites.

To prepare the Pd/PS@ZIF-8@mSiO₂ nanocomposite, the Pd/PS@ZIF-8 nanocomposite was uniformly coated with an amorphous silica shell by a sol-gel process based on the Stöber method. Using tetraethyl orthosilicate (TEOS) as the silica source and hexadecyltrimethylammonium bromide (CTAB) as a soft template, a thin layer was formed around the Pd/PS@ZIF-8 nanocomposite, as shown in Figure 4. The measured thickness of the silica shell was around 30 nm. Therefore, the nanocomposite changed size from 370 nm to 430 nm, clearly indicating that the Pd/PS@ZIF-8@mSiO₂ nanocomposite was successfully coated during the sol-gel process.

Through high-temperature calcination for 5 h, Pd/PS@ZIF-8@mSiO₂ was transformed to the hollow PdO/ZnO@mSiO₂ hybrid nanocatalyst as the final product by removal of the polystyrene core. Moreover, the Pd nanoparticles and ZIF-8 shell were oxidized to PdO nanoparticles and a ZnO shell [28]. In this process, the silica shells help to retain the initial spherical morphology of Pd/PS@ZIF-8@mSiO₂ even after high-temperature calcination. The resulting PdO/ZnO@mSiO₂ hybrid nanocatalyst was characterized by SEM and transmission electron microscopy (TEM). Figure 5 shows the formation of a quite uniform and well-dispersed PdO/ZnO@mSiO₂ nanocomposite with a hollow structure. After oxidation of the organic imidazole and combustion of the polystyrene core, the overall size of the PdO/ZnO@mSiO₂ hybrid nanocatalyst was reduced from 430 to 380 nm.

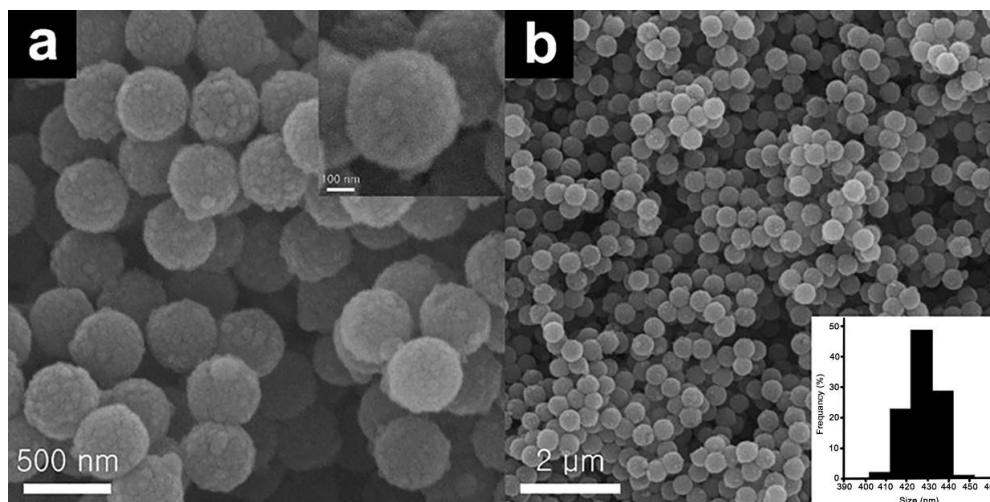


Figure 4. SEM images of Pd/PS@ZIF-8@mSiO₂ nanocomposites (a,b). The insert in (a) is high-resolution SEM image and the insert in (b) is the size distribution of Pd/PS@ZIF-8@mSiO₂ nanocomposites.

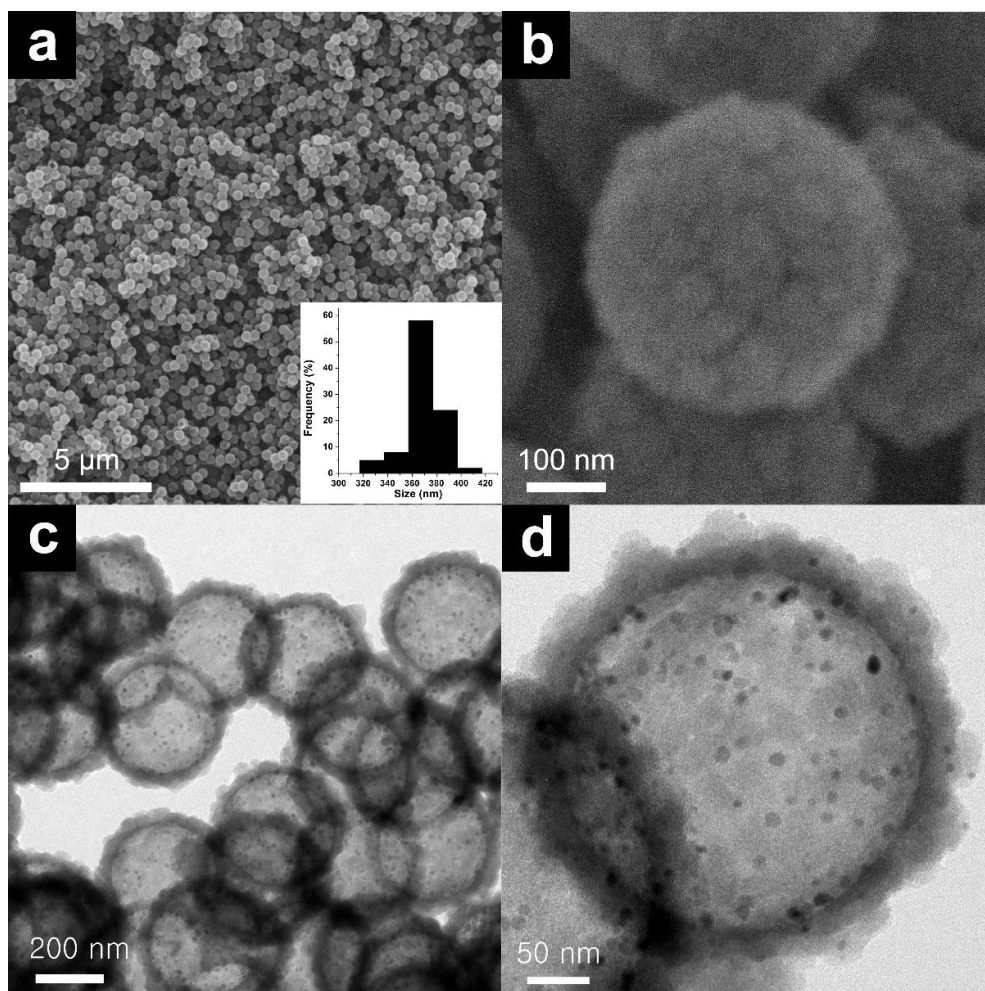


Figure 5. SEM images (a,b) and TEM image (c,d) of PdO/ZnO@mSiO₂ hybrid nanocatalyst. The insert in (a) is the size distribution of PdO/ZnO@mSiO₂ hybrid nanocatalyst.

The PdO/ZnO@mSiO₂ hybrid nanocatalysts were analyzed by N₂ sorption at 77 K. The PdO/ZnO@mSiO₂ hybrid nanocatalyst exhibited type IV adsorption-desorption isotherms, indicating a mesoporous structure (with a pore diameter of 2–50 nm). The Brunauer-Emmett-Teller (BET) surface area and pore size of the nanocomposite were estimated to be 195 m² g⁻¹ and 4.2 nm, respectively. The surface area is higher than that of previously reported ZIF-8-based hollow ZnO@SiO₂ (78 m² g⁻¹) [29]. This result could be attributed to the complete removal of the polystyrene core and transformation of the ZIF-8 shell to the thin ZnO shell.

The PdO/ZnO@mSiO₂ hybrid nanocatalyst was also evaluated using X-ray photoelectron spectroscopy (XPS) and thermogravimetric analysis (TGA; Figure 6). XPS was employed to characterize the oxidation state of Pd, Zn, and Si. The XPS spectra show Pd 3d (Figure 6a), Zn 2p (Figure 6b), and Si 2p (Figure 6c) peaks. The Pd 3d signals were weak due to the low content of palladium, and the binding energy of the Pd 3d_{5/2} XPS peak was about 336.6 eV. In general, the binding energy of Pd 3d_{5/2}, corresponding to Pd(0), is about 335.4 eV, whereas that of PdO is 336.8 eV. Thus, the data indicate that Pd was mainly present in the Pd²⁺ valance state [30]. The observation of an XPS peak for Zn 2p at 1022.9 eV verified that the Zn species existed as ZnO in the PdO/ZnO@mSiO₂ hybrid nanocatalyst because the Zn 2p peak for ZnO generally has a value between 1021 and 1023 eV [31,32]. The Si 2p peak appeared at 103.0 eV and the binding energy of Si 2p matched very well with the reported value [33]. Based on the XPS results, it was found that the PdO/ZnO@mSiO₂ hybrid nanocatalyst comprised PdO, ZnO, and SiO₂.

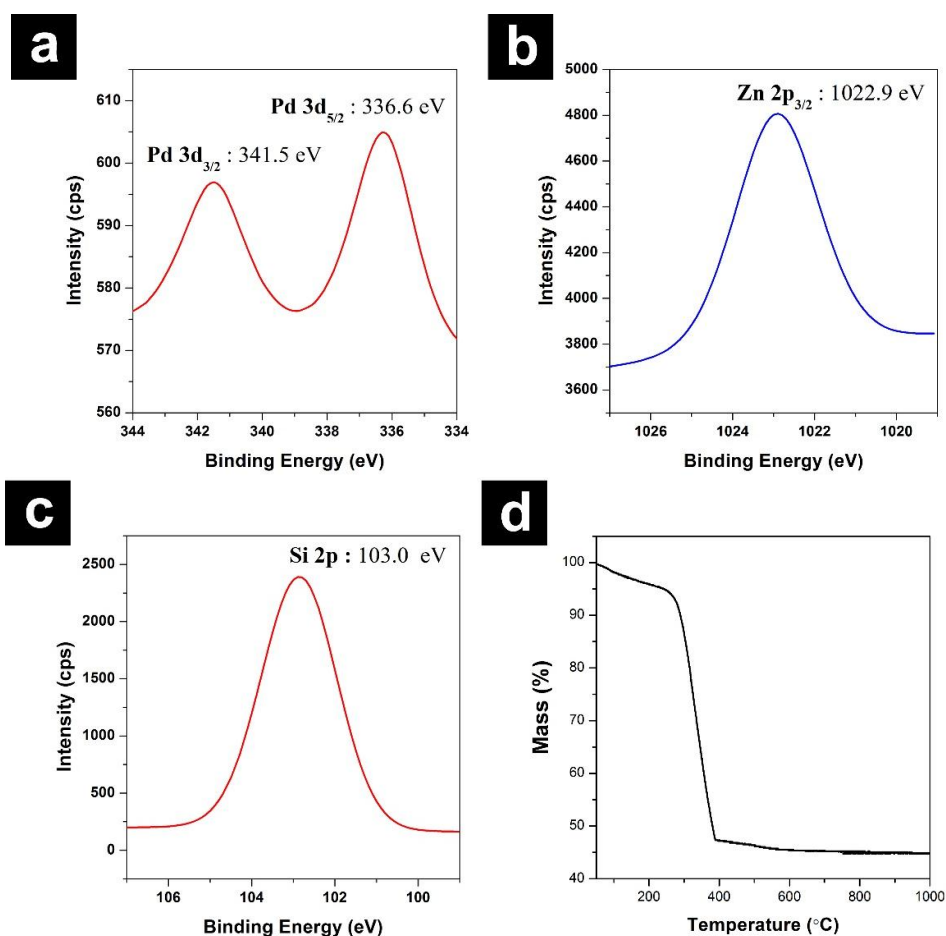


Figure 6. The XPS spectrums (a–c) of PdO/ZnO@mSiO₂ hybrid nanocatalyst and TGA curve (d) of PdO/ZnO@mSiO₂ hybrid nanocatalyst.

The TGA data are shown in Figure 6d. The weight loss of the PdO/ZnO@mSiO₂ hybrid nanocatalyst resulted from the degradation of the polystyrene core and ZIF-8 shell. The polystyrene spheres started to decompose around 280 °C and fully decomposed around 400 °C with 49% loss of weight. The ZIF-8 shell started to decompose around 400 °C, followed by a gradual loss of weight, whereas no significant loss appeared after 620 °C. The data suggest that the PdO/ZnO@mSiO₂ hybrid nanocatalyst exhibits good thermal stability.

2.2. Catalytic Activity of PdO/ZnO@mSiO₂ Hybrid Nanocatalyst

The reduction of nitroarenes with NaBH₄ was conducted to evaluate the catalytic activity of the PdO/ZnO@mSiO₂ hybrid nanocatalyst. As shown in Figure 7, the UV/vis absorption of the reaction mixture was monitored with time to check the progress of the catalytic reduction of 4-NP. 4-NP exhibits a strong absorption peak at 317 nm, and in this reaction, 4-NP is changed to the 4-nitrophenolate ion, which absorbs strongly at 400 nm in the presence of NaBH₄ as a hydrogen source [17]. As the reduction of 4-nitrophenol proceeded in the presence of the catalyst, the absorption of the 4-nitrophenolate ion at 400 nm gradually decreased, whereas the new absorption peak at 298 nm increased due to the formation of 4-AP [34]. As shown in Figure 7a, the absorption peak of the 4-nitrophenolate ion decreased in intensity by only 5% even after 24 h, which indicates that the reduction of 4-NP proceeded quite slowly without the catalyst. Figure 7c shows the reduction of 4-NP to 4-AP using different amounts of catalyst. Upon addition of 5 mol % of the PdO/ZnO@mSiO₂ hybrid nanocatalyst, the absorption at 400 nm decreased rapidly with a concomitant increase in the intensity of the peak at 300 nm within 150 s, which is attributed to the product of the reduction, 4-aminophenol. The reduction was completed in 330 s when 2.5 mol % of the catalyst was used.

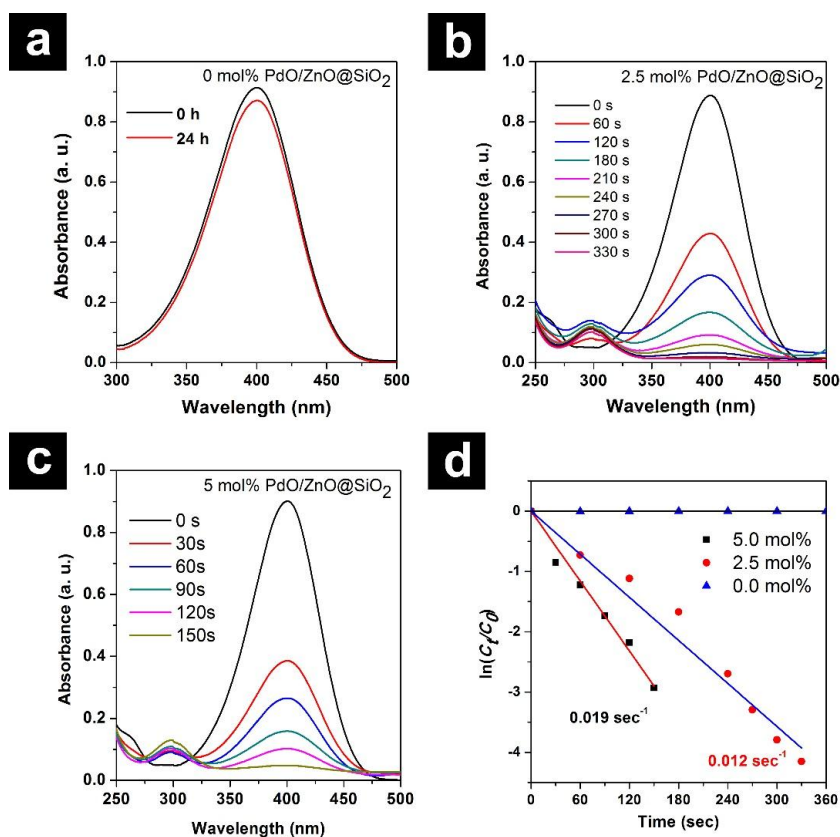


Figure 7. Time-dependent UV-vis absorption spectra for the reduction of 4-NP over different amount of catalyst, 0 mol % (a); 2.5 mol % (b); 5 mol % (c); and Plot of $\ln(C_t/C_0)$ versus time for the reduction of 4-NP with different amount of catalyst (d).

As shown in Figure 7d, the reaction rate constant was also compared as a function of the catalyst loading. The kinetics of reaction could be described by Equation (1):

$$dC_t/dt = -k_{app}C_t \text{ or } \ln(C_t/C_0) = \ln(A_t/A_0) = -k_{app}t \quad (1)$$

Here, A_t and A_0 are the absorbance values of 4-NP measured at time t and $t = 0$, respectively. C and C_0 are the concentration of 4-NP at time t and 0 s, respectively; k_{app} is the apparent rate constant calculated from the reduction in the intensity of the peak at 400 nm with time. The k_{app} for 4-NP reduction with 5 mol % of the PdO/ZnO@mSiO₂ hybrid nanocatalyst was calculated as $1.9 \times 10^{-2} \text{ s}^{-2}$ (Figure 7d). Notably, the catalyst exhibited significantly higher catalytic performance than previously reported catalysts [35–37]. The enhanced catalytic activity of PdO/ZnO@mSiO₂ hybrid nanocatalyst is attributed to the high surface area and the well distribution of small sized PdO NPs on ZnO@mSiO₂ mesoporous hollow structure. The catalytic activity of the PdO/ZnO@mSiO₂ hybrid nanocatalyst was also investigated in the reduction of other nitroarene analogs, as shown in Table 1. The PdO/ZnO@mSiO₂ hybrid nanocatalyst showed high catalytic activity in the reduction of various nitroarenes. Notably, when the reduction of ortho-, para-, and meta-nitroarene was catalyzed by the PdO/ZnO@mSiO₂ hybrid nanocatalyst, meta-nitroarene showed better activity than ortho- and para-nitrophenol. Due to the lack of resonance stabilization, meta-nitroarene is most unstable, and hence more reactive than the ortho- and para analogs. Moreover, the ortho-compound is less stable than the para-compound because of steric effects.

Table 1. Reduction of various nitroarenes using PdO/ZnO@mSiO₂ hybrid nanocatalyst.

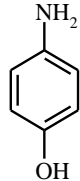
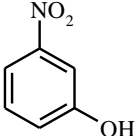
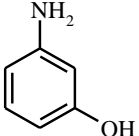
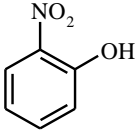
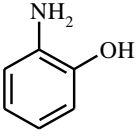
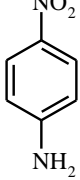
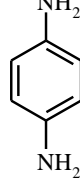
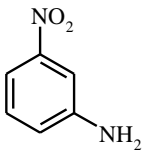
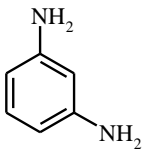
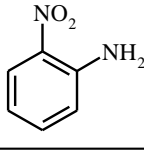
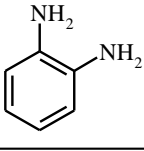
Entry	Substrate	Product	Time (s)	TOF (h ⁻¹)
1			150	480
2			120	600
3			210	343
4			90	800

Table 1. Cont.

Entry	Substrate	Product	Time (s)	TOF (h ⁻¹)
5			45	1600
6			120	600

Reaction condition: 0.71 mM of nitrocompound aqueous solution, 5 mol % of PdO/ZnO@mSiO₂ hybrid nanocatalyst, 1.0 mL of 1.1 M NaBH₄ (150 equiv. to the substrate).

3. Materials and Methods

3.1. General Remarks

Reagents were purchased from Aldrich Chemical Co. (St. Louis, MO, USA), TCI Co. (Tokyo Chemical Industry Co., Ltd., Chuo-ku, Tokyo, Japan), and ACROS Co. (Acros Organics, Geel, Belgium). All chemicals were used as received without any further purification. The particles were characterized by SEM, EDS, TEM, XRD, and XPS. The nanoparticles were characterized by SEM-EDS (FEI, Hillsboro, OR, USA) (FEI Quanta 200 Microscope, 15 kV) and TEM (JEOL JEM-2100F Microscope, 200 kV, JEOL Ltd., Tokyo, Japan). The TEM samples were prepared by putting a few drops of the corresponding colloidal solution on carbon-coated copper grids. XRD patterns were recorded on a Rigaku D/MAX-RD diffractometer (12 kV; Rigaku, Shibuya-ku, Japan). XPS graphs were recorded with a Rigaku D/MAX-RB Co (12 kV; Rigaku, Shibuya-ku, Japan) diffractometer.

3.2. Preparation of Carboxylate-Terminated Polystyrene Nanoparticles (COOH-PS)

The polystyrene nanoparticles were synthesized according to a previously reported method [25,38]. Polymerization was carried out in a 250 mL Schlenk flask with 21 mL of styrene, 0.92 mL of acrylic acid, 1.1 mL of methyl 2-methylpropenoate, and 0.49 g ammonium bicarbonate in 100 mL of deionized water under magnetic stirring at 70 °C. Ammonium persulfate (0.53 g) was then added to the mixture solution. The mixture was stirred for 12 h at 80 °C and a milky polystyrene dispersion was formed. The product was separated by centrifugation and washed three times with deionized water and ethyl alcohol, and then vacuum dried overnight.

3.3. Preparation of Palladium Nanoparticles (Pd NPs) on Polystyrene (Pd/PS)

Pd/PS was synthesized according to a modified reported method [26]. The carboxylate-terminated polystyrene nanoparticles (300 mg) and palladium chloride (30 mg; PdCl₂) were combined in 70 mL of ethyl alcohol and 15 mL of deionized water. The mixture was sonicated for 30 min to dissolve the palladium chloride. Ammonium hydroxide (0.18 mL), as a reducing agent, was added. Separately, 0.5 g of polyvinylpyrrolidone (M_w = 40,000) was dissolved in 10 mL ethyl alcohol. This solution was then added dropwise to the above mixture. After stirring for 12 h at 70 °C, the product was cooled, separated by centrifugation, washed with ethyl alcohol and water, and dried.

3.4. Preparation of Pd/PS@Zeolite Imidazolate Framework (Pd/PS@ZIF-8)

A precursor solution was prepared by mixing 200 mg of Pd/PS nanoparticles and 1.1 g of 2-methylimidazole in 30 mL of methyl alcohol. Zinc nitrate hexahydrate (0.4 g) was separately dissolved in 5 mL methyl alcohol and then added to the precursor solution. This mixture was

refluxed for 20 min at 70 °C, followed by cooling to room temperature. The product was collected by centrifugation, washed with methanol, and dried under vacuum [39].

3.5. Preparation of PdO/ZnO@mSiO₂ Hybrid Nanocatalyst

The as-prepared Pd/PS@ZIF-8 (200 mg) was redispersed via ultrasonication in a mixture of 30 mL ethyl alcohol, 5 mL of deionized water, and 200 mg of cetyltrimethylammonium bromide. Thereafter, 400 µL of tetraethyl orthosilicate was added dropwise to the above mixture, and further stirred for 12 h at 50 °C. After cooling to room temperature, the solid residue was collected by centrifugation and washed with water and ethyl alcohol and dried under vacuum. To obtain the PdO/ZnO@mSiO₂ hybrid nanocatalyst, the Pd/PS@ZIF-8@mSiO₂ was calcined by ramping to 500 °C at a heating rate of 10 °C min⁻¹ for 5 h under air [40].

3.6. Reduction of 4-Nitrophenol Catalyzed by PdO/ZnO@mSiO₂ Hybrid Nanocatalyst

The experiments were performed at room temperature in a 50 mL Schlenk flask. Sodium borohydride solution (1 mL; 1.1 mM) was combined with 10 mL of 4-NP aqueous solution (0.71 mM) under magnetic stirring. Thereafter, 1.43 mg of well dispersed PdO/ZnO@mSiO₂ hybrid nanocatalyst in 1 mL deionized water was added to the above mixture. The yellow color of the 4-nitrophenolate ion solution gradually changed to colorless and transparent. UV-vis spectra were acquired to confirm the color changes of the solution at regular time intervals.

4. Conclusions

A hollow-structured PdO/ZnO@mSiO₂ hybrid nanocatalyst was successfully developed. Palladium oxide nanoparticles and a zinc oxide shell were formed by calcination of the palladium nanoparticles and ZIF-8 in air, respectively. The palladium oxide nanoparticles were easily anchored onto the zinc oxide shell through thermal treatment. Benefitting from their morphology and hybrid nanostructure, the PdO/ZnO@mSiO₂ hybrid nanocatalyst exhibited superior catalytic activity for the reduction of nitroarenes under eco-friendly conditions. A loading of 5 mol % of the PdO/ZnO@mSiO₂ hybrid nanocatalyst led to a high reaction rate constant of up to $1.9 \times 10^{-2} \text{ s}^{-2}$ for 4-nitrophenol reduction. The present strategy affords a new synthesis method for the preparation of several silica microsphere@metal support catalysts with dense metallic nanoshells, which may in turn be utilized for other catalytic reactions and applications.

Author Contributions: J.K. conceived and designed the experiments; J.K., A.K. and N.M. performed the experiments and analyzed the data; J.K., N.M. and K.H.P. wrote the paper; K.H.P. supervised the research.

Funding: 2-Year Research Grant of Pusan National University.

Acknowledgments: This work was supported by a 2-Year Research Grant of Pusan National University.

Conflicts of Interest: The authors declare no conflict of interest.

References

1. Xia, Y.; Yang, H.; Campbell, C.T. Nanoparticles for catalysis. *Acc. Chem. Res.* **2013**, *46*, 1671–1672. [[CrossRef](#)] [[PubMed](#)]
2. Duan, X.; Liu, J.; Hao, J.; Wu, L.; He, B.; Qiu, Y.; Zhang, J.; He, Z.; Xi, J.; Wang, S. Magnetically recyclable nanocatalyst with synergetic catalytic effect and its application for 4-nitrophenol reduction and Suzuki coupling reactions. *Carbon* **2018**, *130*, 806–813. [[CrossRef](#)]
3. Gawande, M.B.; Goswami, A.; Felpin, F.X.; Asefa, T.; Huang, X.; Silva, R.; Zou, X.; Zboril, R.; Varma, R.S. Cu and Cu-based nanoparticles: Synthesis and applications in catalysis. *Chem. Rev.* **2016**, *116*, 3722–3811. [[CrossRef](#)] [[PubMed](#)]
4. Jang, S.; Kim, T.; Park, K.H. Fabrication of crumpled ball-like nickel doped palladium-iron oxide hybrid nanoparticles with controlled morphology as effective catalyst for Suzuki–Miyaura coupling reaction. *Catalysts* **2017**, *7*, 247. [[CrossRef](#)]

5. Woo, H.; Park, J.; Yun, S.W.; Park, J.C.; Park, S.; Kim, Y.T.; Park, K.H. Shape-controlled synthesis of dumbbell-like Pt-Fe₃O₄-MnO_x nanoparticles by governing the reaction kinetics. *ACS Omega* **2017**, *2*, 8483–8489. [CrossRef]
6. Gopalan, A.I.; Muthuchamy, N.; Komathi, S.; Lee, K.P. A novel multicomponent redox polymer nanobead based high performance non-enzymatic glucose sensor. *Biosens. Bioelectron.* **2016**, *84*, 53–63. [CrossRef] [PubMed]
7. Venugopal, A.; Muthuchamy, N.; Tejani, H.; Gopalan, A.I.; Lee, K.P.; Lee, H.J.; Kyung, H.M. Incorporation of silver nanoparticles on the surface of orthodontic microimplants to achieve antimicrobial properties. *Korean J. Orthod.* **2017**, *47*, 3–10. [CrossRef] [PubMed]
8. Navalón, S.; García, H. Nanoparticles for catalysis. *Nanomaterials* **2016**, *6*, 123. [CrossRef] [PubMed]
9. Kim, M.; Park, J.C.; Kim, A.; Park, K.H.; Song, H. Porosity Control of Pd@SiO₂ Yolk-Shell nanocatalysts by the formation of nickel phyllosilicate and its influence on Suzuki coupling reactions. *Langmuir* **2012**, *28*, 6441–6447. [CrossRef] [PubMed]
10. Atchudan, R.; Edison, T.N.J.I.; Perumal, S.; Shanmugam, M.; Lee, Y.R. Direct solvothermal synthesis of zinc oxide nanoparticle decorated graphene oxide nanocomposite for efficient photodegradation of azo-dyes. *J. Photochem. Photobiol. A* **2017**, *337*, 100–111. [CrossRef]
11. Dong, W.; Cheng, S.; Feng, C.; Shang, N.; Gao, S.; Wang, C. Fabrication of highly dispersed Pd nanoparticles supported on reduced graphene oxide for catalytic reduction of 4-nitrophenol. *Catal. Commun.* **2017**, *90*, 70–74. [CrossRef]
12. Muthuchamy, N.; Atchudan, R.; Edison, T.N.J.I.; Perumal, S.; Lee, Y.R. High-performance glucose biosensor based on green synthesized zinc oxide nanoparticle embedded nitrogen-doped carbon sheet. *J. Electroanal. Chem.* **2018**, *816*, 195–204. [CrossRef]
13. Cai, R.; Ellis, P.R.; Yin, J.; Liu, J.; Brown, C.M.; Griffin, R.; Chang, G.; Yang, D.; Ren, J.; Cooke, K.; et al. Performance of preformed Au/Cu nanoclusters deposited on MgO powders in the catalytic reduction of 4-nitrophenol in solution. *Small* **2018**, *14*, 1703734. [CrossRef] [PubMed]
14. Xia, J.; Fu, Y.; He, G.; Sun, X.; Wang, X. Core-shell-like Ni-Pd nanoparticles supported on carbon black as a magnetically separable catalyst for green Suzuki-Miyaura coupling reactions. *Appl. Catal. B-Environ.* **2017**, *200*, 39–46. [CrossRef]
15. Kim, A.; Muthuchamy, N.; Yoon, C.; Joo, S.H.; Park, K.H. MOF-derived Cu@Cu₂O nanocatalyst for oxygen reduction reaction and cycloaddition reaction. *Nanomaterials* **2018**, *8*, 138. [CrossRef] [PubMed]
16. Jang, S.; Yoon, C.; Lee, J.M.; Park, S.; Park, K.H. Preparation of Cu@Cu₂O nanocatalysts by reduction of HKUST-1 for oxidation reaction of catechol. *Molecules* **2016**, *21*, 1467. [CrossRef] [PubMed]
17. Muthuchamy, N.; Gopalan, A.; Lee, K.P. A new facile strategy for higher loading of silver nanoparticles onto silica for efficient catalytic reduction of 4-nitrophenol. *RSC Adv.* **2015**, *5*, 76170–76181. [CrossRef]
18. Kim, A.; Bae, H.S.; Park, J.C.; Song, H.; Park, K.H. Surfactant-free Pd@pSiO₂ yolk-shell nanocatalysts for selective oxidation of primary alcohols to aldehydes. *New J. Chem.* **2015**, *39*, 8153–8157. [CrossRef]
19. Nallal, M.; Anantha Iyengar, G.; Pill-Lee, K. New titanium dioxide-based heterojunction nano-hybrid for highly selective photoelectrochemical-electrochemical dual-mode sensors. *ACS Appl. Mater. Interfaces* **2017**, *9*, 37166–37183. [CrossRef] [PubMed]
20. Lou, X.W.D.; Archer, L.A.; Yang, Z. Hollow micro-/nanostructures: Synthesis and applications. *Adv. Mater.* **2008**, *20*, 3987–4019. [CrossRef]
21. Yan, Z.; Fu, L.; Zuo, X.; Yang, H. Green assembly of stable and uniform silver nanoparticles on 2D silica nanosheets for catalytic reduction of 4-nitrophenol. *Appl. Catal. B-Environ.* **2018**, *226*, 23–30. [CrossRef]
22. Polshettiwar, V.; Len, C.; Fihri, A. Silica-supported palladium: Sustainable catalysts for cross-coupling reactions. *Coord. Chem. Rev.* **2009**, *253*, 2599–2626. [CrossRef]
23. Ni, D.; Jiang, D.; Ehlerding, E.B.; Huang, P.; Cai, W. Radiolabeling Silica-Based Nanoparticles via Coordination Chemistry: Basic Principles, Strategies, and Applications. *Acc. Chem. Res.* **2018**, *51*, 778–788. [CrossRef] [PubMed]
24. EPA. 2008, Water Quality Standard Base EPA Numeric Criteria Report. Available online: http://iaspub.epa.gov/waters10/rpt_epa_num_criteria.run_report (accessed on 17 July 2008).
25. Carné-Sánchez, A.; Imaz, I.; Cano-Sarabia, M.; Maspoch, D. A spray-drying strategy for synthesis of nanoscale metal-organic frameworks and their assembly into hollow superstructures. *Nat. Chem.* **2013**, *5*, 203. [CrossRef] [PubMed]

26. Cheng, X.; Tjong, S.C.; Zhao, Q.; Li, R.K.Y. Facile method to prepare monodispersed Ag/polystyrene composite microspheres and their properties. *J. Polym. Sci. Part A Polym. Chem.* **2009**, *47*, 4547–4554. [[CrossRef](#)]
27. Cravillon, J.; Muzer, S.; Lohmeier, S.J.; Feldhoff, A.; Huber, K.; Wiebcke, M. Rapid room-temperature synthesis and characterization of nanocrystals of a prototypical zeolitic imidazolate framework. *Chem. Mater.* **2009**, *21*, 1410. [[CrossRef](#)]
28. Du, Y.; Chen, R.Z.; Yao, J.F.; Wang, H.T. Facile fabrication of porous ZnO by thermal treatment of zeolitic imidazolate framework-8 and its photocatalytic activity. *J. Alloys Compd.* **2013**, *551*, 125–130. [[CrossRef](#)]
29. He, L.; Li, L.; Zhang, L.; Xing, S.; Wang, T.; Li, G.; Wang, C. ZIF-8 templated fabrication of rhombic dodecahedron-shaped ZnO@SiO₂, ZIF-8@SiO₂ yolk-shell and SiO₂ hollow nanoparticles. *CrystEngComm* **2014**, *16*, 6534–6537. [[CrossRef](#)]
30. Brun, M.; Berthet, A.; Bertolini, J.C. XPS, AES and Auger parameter of Pd and PdO. *J. Electron Spectrosc. Relat. Phenom.* **1999**, *104*, 55–60. [[CrossRef](#)]
31. Mulligan, R.F.; Iliadis, A.A.; Kofinas, P. Synthesis and characterization of ZnO nanostructures templated using diblock copolymers. *J. Appl. Polym. Sci.* **2003**, *89*, 1058–1061. [[CrossRef](#)]
32. Tay, Y.Y.; Li, S.; Sun, C.Q.; Chen, P. Size dependence of Zn 2p 3/2 binding energy in nanocrystalline ZnO. *Appl. Phys. Lett.* **2006**, *88*, 173118. [[CrossRef](#)]
33. Kanungo, J.; Selegård, L.; Vahlberg, C.; Uvdal, K.; Saha, H.; Basu, S. XPS study of palladium sensitized nano porous silicon thin film. *Bull. Mater. Sci.* **2010**, *33*, 647–651. [[CrossRef](#)]
34. Kang, H.; Kim, M.; Park, K.H. Effective immobilization of gold nanoparticles on core-shell thiol-functionalized GO coated TiO₂ and their catalytic application in the reduction of 4-nitrophenol. *Appl. Catal. A-Gen.* **2015**, *502*, 239–245. [[CrossRef](#)]
35. Xia, Y.; Gao, Z.; Liao, X.; Yan, S.; Han, J.; Wang, X.; Pan, C.; Zhang, Y.; Zhai, W. One-step green synthesis of silver nanobelts assisted by sodium carboxymethylcellulose for catalytic reduction of 4-nitrophenol. *CrystEngComm* **2018**, *20*, 2135–2143. [[CrossRef](#)]
36. Wu, W.; Lei, M.; Yang, S.; Zhou, L.; Liu, L.; Xiao, X.; Jiang, C.; Roy, V.A. A one-pot route to the synthesis of alloyed Cu/Ag bimetallic nanoparticles with different mass ratios for catalytic reduction of 4-nitrophenol. *J. Mater. Chem. A* **2015**, *3*, 3450–3455. [[CrossRef](#)]
37. Min, J.; Wang, F.; Cai, Y.; Liang, S.; Zhang, Z.; Jiang, X. Azeotropic distillation assisted fabrication of silver nanocages and their catalytic property for reduction of 4-nitrophenol. *Chem. Commun.* **2014**, *51*, 761–764. [[CrossRef](#)] [[PubMed](#)]
38. Haes, A.J.; Hall, W.P.; Chang, L.; Klein, W.L.; Van Duyne, R.P. A localized surface plasmon resonance biosensor: First steps toward an assay for Alzheimer's disease. *Nano Lett.* **2004**, *4*, 1029–1034. [[CrossRef](#)]
39. Lee, H.J.; Won, C.; Oh, M. Advanced fabrication of metal-organic frameworks: Template-directed formation of polystyrene@ ZIF-8 core-shell and hollow ZIF-8 microspheres. *Chem. Commun.* **2012**, *48*, 221–223. [[CrossRef](#)] [[PubMed](#)]
40. Guo, X.; Deng, Y.; Gu, D.; Che, R.; Zhao, D.; Guo, X. Synthesis and microwave absorption of uniform hematite nanoparticles and their core-shell mesoporous silica nanocomposites. *J. Mater. Chem.* **2009**, *19*, 6706–6712. [[CrossRef](#)]

